Solubility in Supercritical Carbon Dioxide: Importance of the Poynting Correction and Entrainer Effects

Kelly E. Anderson and J. Ilja Siepmann*

Department of Chemistry and Department of Chemical Engineering and Materials Science, University of Minnesota, 207 Pleasant St. SE, Minneapolis, Minnesota 55455-0431

Received: March 18, 2008; Revised Manuscript Received: June 16, 2008

Gibbs ensemble Monte Carlo simulations were used to investigate the effect of pressure and of entrainers on the solubility of low-volatility species in CO_2. Two entrainers were examined, *n*-octane and methanol, as well as two solutes, hexamethylbenzene and benzoic acid. For the three pressures studied (12, 20, and 28 MPa), the simulations demonstrate that the increase in the solubility with increasing pressure is mostly due to an increase in the solute's chemical potential (as expressed by the Poynting correction) and not due to an increase in the solvent strength of supercritical CO_2. The presence of an entrainer enhances solubility, particularly when the solute and entrainer can form hydrogen bonds. The solubility of benzoic acid is enhanced by an order of magnitude upon addition of methanol entrainer, whereas the enhancements are less than 2 for the other systems.

1. Introduction

Supercritical (SC) fluids are attractive solvents for a variety of applications because of their unique properties, particularly the ability to adjust the solvent strength by changing the temperature or presssure.[1−4] Many common applications exploit this property, including SC fluid extraction and chromatography. Carbon dioxide (CO_2) is a particularly useful SC fluid as it is nontoxic and nonflammable and has a readily accessible critical point ($T = 304.3$ K, $p = 73.8$ bar).

One of the limitations of using SC fluids is the low solubility of many organic species compared to traditional liquid solvents. This is particularly true of polar species.[5,6] The use of entrainers, also referred to as cosolvents or modifiers, has been examined extensively as a means to enhance the solubility of organic species in SC fluids.[4−7] Among these studies are those of Dobbs et al. on the solubility enhancement effects of polar and nonpolar entrainers in SC-CO_2.[5,6] In the near-critical region, they exploit density and polarity effects to enhance solubility by as much as a factor of 7. Overall, changes in density of the SC phase result in only slight changes in solubility, while adjusting the polarity of the entrainer can have a substantial impact on solute solubility, particularly for polar solutes.[5,6]

While molecular simulations have been used extensively to examine the phase behavior, microscopic structure, and transport properties of binary SC-CO_2 systems[9−17] and the solubility of solid solutes in SC-CO_2,[18−29] there have been few studies of ternary solute/CO_2/entrainer mixtures.[30−33] The aim of this work is to investigate these ternary mixtures, particularly the factors influencing solubility in neat and cosolvent-enriched SC-CO_2. Monte Carlo simulations are used to examine the effect of *n*-octane (OCT) and methanol (MeOH) cosolvents on the solubility of hexamethylbenzene (HMB) and benzoic acid (BA) in SC-CO_2 over a range of pressures.

* Corresponding author: E-mail: siepmann@umn.edu.

2. Molecular Models

The site−site interactions of solvent, solute, and entrainer are described by the pairwise additive 12−6 Lennard-Jones (LJ) potential and Coulombic potential with fixed point charges

$$u(r_{ij}) = 4\epsilon_{ij}\left[\left(\frac{\sigma_{ij}}{r_{ij}}\right)^{12} - \left(\frac{\sigma_{ij}}{r_{ij}}\right)^{6}\right] + \frac{q_i q_j}{4\pi\epsilon_0 r_{ij}} \quad (1)$$

where r_{ij}, ϵ_{ij}, σ_{ij}, q_i and q_j are the separation, LJ well depth, LJ diameter, and partial charges for the pair of interaction sites i and j, respectively, and ϵ_0 is the permittivity of vacuum. The LJ parameters and partial point charges were taken from the transferable potentials for phase equilibria (TraPPE) force field,[34−38] with the exception of the acid group of BA for which the parameters were taken from the OPLS force field.[39] The TraPPE force field is fitted to vapor−liquid coexistence data and has been shown to accurately reproduce the phase behavior of CO_2 and its mixtures with alkanes and MeOH.[14,35,40]

Carbon dioxide is treated as a rigid molecule with three interaction sites. The united-atom version of the TraPPE force field is used to represent the methyl, methylene, and aromatic methine units. This results in eight and three interaction sites for OCT and MeOH, respectively. For both HMB and BA, the benzene rings were modeled with the six-site TraPPE potential,[37] where one site is located at each sp^2 C or CH site. The standard Lorentz−Berthelot combining rules were used to determine interaction parameters for unlike sites.[41] A spherical potential trucation was used ($r_{cut} = 14$ Å) along with analytic tail corrections for the LJ interactions and the Ewald sum for long-range Coulombic interactions.[42]

While CO_2, HMB, and the phenyl ring of BA are treated as fully rigid, the other molecules and the BA headgroup are treated as semirigid and allowed to sample different conformations. All bond lengths are fixed at their equilibrium values. A harmonic bending potential and a cosine series dihedral potential are used to govern bond angle bending and, if present, dihedral motion for MeOH, OCT, and the carboxylic headgroup of BA.

10.1021/jp802374c CCC: $40.75
Published on Web 08/16/2008

3. Simulation Details

Simulations were performed in a variant of the isobaric−isothermal Gibbs ensemble[43−47] using periodic boundary conditions at three different pressures (12, 20, and 28 MPa). The supercritical phase was modeled by one box, while the second modeled the saturated vapor phase of the solute. This was done in order to avoid explicitly simulating the crystalline phase of the solute and thereby increasing the complexity of the simulation. The pressure of the solute box was set to the saturated vapor pressure of the solute. Both boxes were kept at 310 K, which is slightly above the temperature used in previous experimental studies (308 K)[5,6] but consistent with the slightly elevated critical temperature of TraPPE-CO_2 (306 K).[35] Only the solute molecules were allowed to transfer between the phases, whereas CO_2 and the entrainers were confined to the SC box. The supercritical phase was composed of 2000 solvent molecules. In the cosolvent systems, the number of CO_2 molecules was decreased to 1930 while 70 entrainer molecules were added (3.5 mol %) to keep the total number of solvent molecules constant. Initially, 30 solute molecules were present in the vapor phase, except for the BA/CO_2 /MeOH system where 60 solute molecules were used.

Four independent simulations were performed for each state point, starting from different initial configurations. The systems were allowed to equilibrate for at least 5×10^4 cycles followed by at least 10^5 cycles of production (where a cycle consists of N randomly selected Monte Carlo moves). Statistical uncertainties were estimated from the four independent simulations. In addition to the standard translation and rotation moves used for all molecule types, coupled−decoupled configurational-bias Monte Carlo moves[48,49] were used for particle insertions/deletions and to sample the conformational space of OCT, MeOH, and the carboxylic acid headgroup of BA. Each simulation box was brought into equilibrium with the applied external pressure using volume moves.[50] Aggregation-volume-bias[51,52] moves were used to facilitate cluster formation and destruction for MeOH and BA.

4. Results and Discussion

A. Pressure Effects on Solubility Isotherms. Initially, the simulations were performed with the external pressure of the vapor box equal to the experimentally determined saturated vapor pressure of the solids at 308 K (HMB, 0.49 Pa;[53] BA, 0.35 Pa[54]). Using these vapor pressures (or solute chemical potentials), the mole fractions of solute, x_{solute}, in the SC phase obtained from the simulations are significantly smaller than the experimental concentrations[5,6] (see Figure 1). Although the calculated x_{BA} increases slightly (by ≈15%) upon increasing the pressure of the SC phase from 12 to 28 MPa, the calculated x_{HMB} decreases by nearly 40%. In contrast, the experimental data show an increase in solubility with increasing pressure.

Thus, assuming that the external pressure has a negligible effect on the vapor pressure of the solid (or that the chemical potential of the solid remains constant) does not yield the correct solubility behavior. The effect of the external pressure on the saturated vapor pressure of the solid can be taken into account via the Poynting correction.[55] The Poynting correction takes the form

$$p^{corr} = p^{coex} \exp\left[\int_{p^{coex}}^{p^{ext}} \frac{V_m}{RT}\, dp\right] \quad (2)$$

where p^{coex}, p^{ext}, V_m, R, and T are the saturated vapor pressure of the neat solid, the applied (or external) pressure, the molar volume of the solid, the molar gas constant, and absolute temperature, respectively. If the vapor phase is treated as an ideal gas and V_m is assumed to remain constant over the given pressure range, eq 2 can be simplified as

$$p^{corr} = p^{coex} \exp(V_m \Delta p/RT) \quad (3)$$

where Δp is the difference between p^{ext} and p^{coex}.

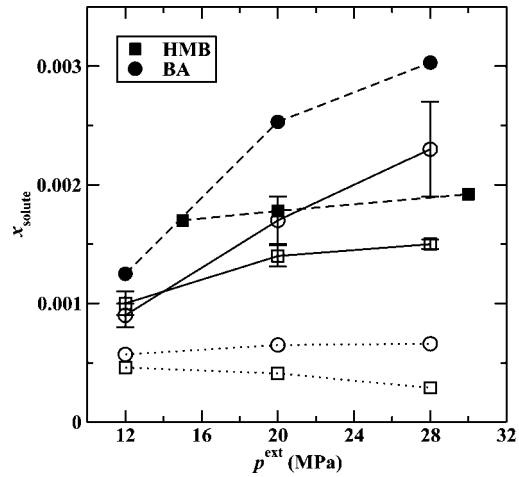

Figure 1. Solubility isotherms for HMB and BA systems in pure CO_2. Filled symbols with dashed lines are the experimental data.[5,6] Simulation results are indicated by open symbols with the Poynting correction to the vapor pressure (solid lines) and without (dotted lines). The error bars indicate the standard error of the mean and are only shown for data sets where the error exceeds the symbol size. The lines are provided as a guide to the eye.

TABLE 1: Poynting Corrected Vapor Pressures, Pressure Ratios, Solubility Ratios, and Partition Constants for HMB and BA[a]

molecule	p^{ext} (MPa)	p^{corr} (Pa)	p^{corr}/p^{coex}	$x^{corr}_{solute}/x^{coex}_{solute}$	K_{trans} (10^4)
HMB	12	1.05	2.1	2.2_3	4.4_4
	20	1.71	3.5	3.4_3	4.1_3
	28	2.81	5.7	5.3_7	3.0_3
BA	12	0.57	1.6	1.6_2	8_1
	20	0.78	2.2	2.6_4	11_2
	28	1.08	3.1	3.5_6	12_2

[a] Subscripts denote the standard error of the mean.

At the high pressures used for SC fluid extractions, the Poynting correction to the vapor pressure cannot be considered negligible. The adjusted vapor pressures for each solute are given in Table 1, and the p^{corr} values for HMB are increased by a factors of about 2 and 6 compared to p^{coex} for $p^{ext} = 12$ and 28 MPa, respectively. Due to its smaller V_m, the increases are smaller for BA. Once the Poynting corrections are applied, the solubilities obtained from the simulations are in much better agreement with the experimental data[5,6] (see Figure 1 and Table 2). The dramatic change upon using the Poynting correction indicates that the increasing solubility is not simply caused by changes in the density of SC-CO_2.

To quantify the importance of the Poynting correction, the numerical values for the ratios of the solid vapor pressure and solubility are listed in Table 1 and their correlation is indicated in Figure 2. The correlation is very good with a slope of 0.93 ± 0.14 and a goodness of the weighted linear fit of 0.90.[56] Thus, the Henry's law like behavior observed in the simulations demonstrates that the change in the chemical potential of the solute is much more important than the change in the density of SC-CO_2 for driving the solubilty increase with increasing pressure. Similarly, we concluded previously that for SC fluid

TABLE 2: Supercritical Phase Solute Mole Fractions and Solubility Enhancements Obtained from Simulation (with Poynting Correction) and Experiment[5,6] [a]

	x_{solute} (10^3)		CISE	
p^{ext} (MPa)	sim	expt	sim	expt
HMB				
12	1.00_{10}	1.70 (15)		
20	1.40_{9}	1.78		
28	1.54_{4}	1.92 (30)		
HMB/OCT				
12	1.70_{10}	3.00	1.7_{2}	1.8
20	1.88_{8}	3.50	1.3_{1}	2.0
28	1.93_{16}	3.71 (30)	1.3_{1}	1.9
HMB/MeOH				
12	1.09_{10}	1.63	1.1_{2}	1.0
20	1.41_{9}	2.11	1.0_{1}	1.2
28	1.54_{12}	2.21 (35)	1.0_{1}	1.2
BA				
12	0.90_{7}	1.25		
20	1.66_{24}	2.53		
28	2.34_{37}	3.03		
BA/OCT				
12	1.31_{17}	2.90 (10)	1.5_{2}	2.3
20	2.16_{29}	5.55 (25)	1.3_{3}	2.2
28	2.02_{86}	5.82 (30)	0.9_{4}	1.9
BA/MeOH				
12	18.6_{22}	7.18	20_{3}	5.7
20	19.4_{11}	10.1	12_{2}	4.0
28	21.7_{9}	11.2 (30)	9_{2}	3.7

[a] If the experimental data was not taken at the pressure indicated, the experimental pressure is shown in parentheses. Subscripts denote the standard error of the mean.

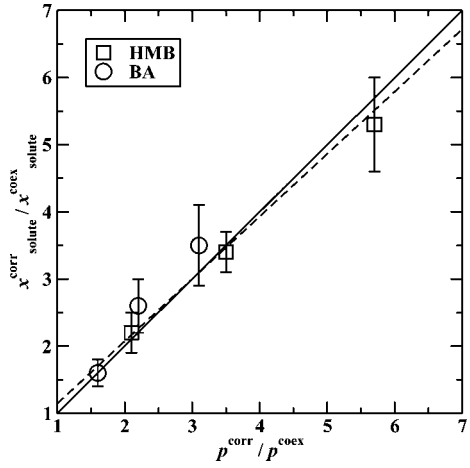

Figure 2. Correlation plot of the solubility ratio versus the vapor pressure ratio upon application of the Poynting correction. The solid line shows an ideal correlation and the dashed line is a weighted linear fit to the simulation data. The error bars indicate the standard error of the mean.

extraction of a liquid, the swelling of the liquid solute-rich phase (i.e., the destabilization of the solute phase) contributes significantly to its increasing solubility in the SC phase.[57]

The partition coefficients, K_{trans}, for the solute transfer from the vapor phase at p^{corr} to the SC phase at p^{ext} are also listed in Table 1. On the basis of the linear correlation between the ratios of the solid's vapor pressure and solubility, one would expect the values of K_{trans} to be nearly constant as the pressure changes. Indeed, the changes in K_{trans} are found to be relatively small while the magnitude of K_{trans} is quite large; i.e., the solutes show a strong preference for the SC phase. For HMB, K_{trans} decreases with increasing p^{ext}. This is expected because upon increasing p^{ext} from 12 to 28 MPa, p^{corr} increases by a factor of 2.7, whereas x_{solute} increases only by a factor of 1.5 (see Table 2; the experiments[5] yield a smaller increase of 1.13 upon increasing p^{ext} from 15 to 30 MPa). In contrast, the value of K_{trans} for BA is found to increase with increasing p^{ext}. Presumably, because the stronger dipole−quadrupole interactions between BA and CO_2 can overcome the entropic cost of cavity formation into the denser SC phase. Correspondingly, both the simulations and experiment show an increase of x_{solute} by a factor of ≈2.5 upon increasing p^{ext} from 12 to 28 MPa (see Table 2).

B. Entrainer Effects on Solubility Isotherms. The effect of entrainers on solute solubility is evident from the data summarized in Table 2. The simulations show that the addition of MeOH entrainer has the greatest effect on the solubility of BA, where the ratio of the solute mole fraction in the ternary and binary systems, called the cosolvent-induced solubility enhancement (CISE), is 12 ± 2 at the intermediate pressure (20 MPa). The experimental measurements also show the largest CISE for this system but give a smaller value of 4 at 20 MPa.[6] When nonpolar OCT is added to SC-CO_2, the calculated solubilities of HMB and BA are slightly increased, e.g., the CISE is 1.3 for both at 20 MPa. The experiments also find a modest effect with CISE values close to 2 over the entire pressure range.[6] Both experiment and simulation show that addition of MeOH entrainer has a negligible effect on the solubility of HMB.[6]

With respect to pressure, we find that the CISE values are always highest at the lowest p^{ext} (12 MPa). However, with the exception of the CISE for BA in the presence of MeOH, where the difference between lowest and highest pressure is about a factor of 2, the pressure effects on the CISEs are small. The experimental data also show CISEs that are insensitive to pressure with the exception of BA with MeOH entrainer where the CISE is about a factor of 1.6 higher at 12 MPa than at 30 MPa.[5,6]

A comparison of the absolute x_{solute} values between experiment and simulation shows that the latter underestimates x_{solute} in SC-CO_2 without and with entrainer by about 30% with the exceptions of BA with entrainer that are substantially underestimated for OCT and overestimated for MeOH.

C. Radial Distribution Functions. Figure 3 shows the radial distribution functions (RDF) and number integrals (NI) for the methyl groups of HMB with varying solvent/entrainer sites. The CH_3(HMB)–C(CO_2) RDFs and NIs are very similar irrespective whether an entrainer is present or not, and only those for the neat SC-CO_2 solvent are depicted. The solute−solvent RDF shows a slight peak at $r \approx 4.5$ Å, and the effect of pressure is very small with slightly more structuring at the lowest p^{ext}. The corresponding NI increases smoothly with distance such that approximately 22 CO_2 molecules are within 8 Å of a solute methyl group.

When the solvent phase is modified by OCT, very few structural features are evident in the CH_3(HMB)–CH_3(OCT) RDF with a very weak peak at $r \approx 4.6$ Å. The CH_3(HMB)–CH_3(MeOH) RDF shows only a slightly stronger peak at $r \approx 4.5$ Å, indicating that any specific interactions between HMB and MeOH are also very weak. Examining the corresponding NIs with CH_3 (OCT) and with CH_3 (MeOH), one finds values of 1.6 and 0.75, respectively, at $r = 8$ Å ($p^{ext} = 20$ MPa), i.e., after accounting for the fact that OCT possesses two CH_3 groups the extent of specific clustering of OCT around HMB does not significantly exceed that of MeOH around HMB.

In contrast, the BA systems show very different pair correlation behavior between the nonpolar and polar entrainer

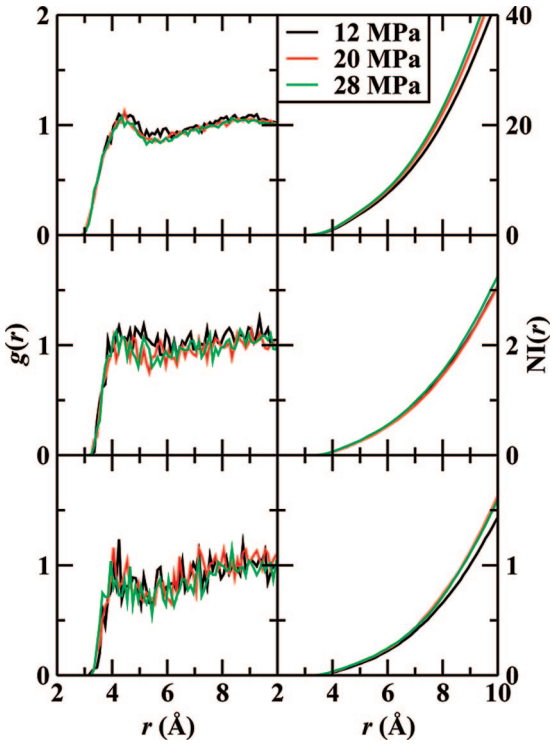

Figure 3. Site−site RDFs and NIs for the methyl groups of HMB and solvent/entrainer sites: $C(CO_2)$ in SC-CO_2 without entrainer, CH_3(OCT), and CH_3(MeOH) are shown at top, middle, and bottom, respectively. NIs are shown for solvent/entrainer sites around the solute's methyl groups.

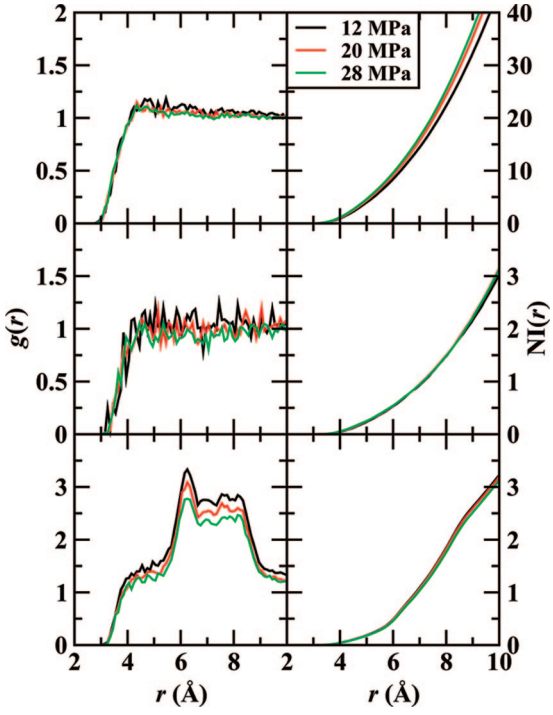

Figure 4. Site−site RDFs and NIs for the aromatic CH groups of BA and solvent/entrainer sites: $C(CO_2)$ in SC-CO_2 without entrainer, CH_3(OCT), and CH_3(MeOH) are shown at top, middle, and bottom, respectively. NIs are shown for solvent/entrainer sites around the solute's CH groups.

systems. Figure 4 shows the site−site RDFs and NIs for the same solvent/entrainer groups with the five aromatic CH groups on the phenyl ring. Here, it should be noted that the 5 CH groups are not identical because of the presence of the carboxylic group.

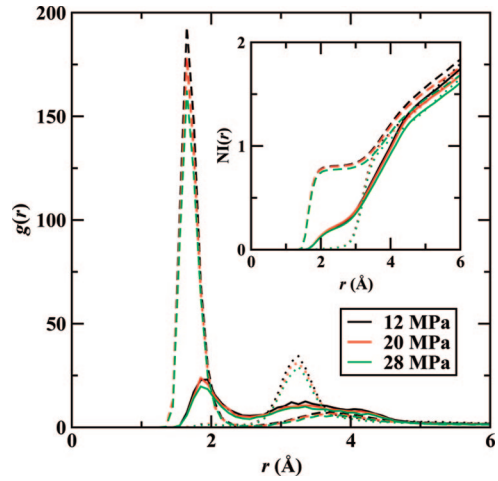

Figure 5. Site−site RDFs and NIs for interactions of polar groups at p^{ext} = 20 MPa: carbonyl O(BA)–H(MeOH), hydroxyl O(BA)–H(MeOH), and H(BA)–O(MeOH) are shown as solid, dotted, and dashed lines, respectively. NIs are shown for entrainer sites around solute sites.

Nevertheless, these RDFs and NIs are averaged over all CH groups to improve the statistics. The CH(BA)–$C(CO_2)$ RDF is slightly less structured than the corresponding RDF for HMB; i.e., there is a small difference in the solvation of the solute's methyl and aromatic CH groups. On the other hand, the CH(BA)–CH_3(OCT) RDF is very similar to that for CH_3 (HMB). However, most significant is the change in the RDFs and NIs with CH_3(MeOH). In this case, the CH(BA)–CH_3(MeOH) RDFs show a shoulder from r = 4 to 5.5 Å, followed by a peak centered at 6.2 Å and a plateau extending to 8.5 Å (again, the heights of the peaks are shifted upward for the lowest pressure). This somewhat unusual RDF shape can be deconvoluted by considering the different types of CH(BA) groups. The peak at 6.2 Å arises mostly from interactions with CH groups in positions 2 and 6 on the phenyl ring, while the CH groups in positions 3 to 5 make the predominant contribution to the plateau. Thus, this unusual peak is clearly associated with specific interactions of the BA's carboxylic group with MeOH. Furthermore, the NI values at r = 8 Å show 1.7 CH_3 (MeOH) versus 1.4 CH_3 (OCT) groups, i.e., indicating preferential solvation particularly after accounting for the fact that OCT possesses twice as many CH_3 groups.

The RDFs and NIs for the polar groups of BA and the MeOH entrainer are depicted in Figure 5. By far the most pronounced is the first peak for the interaction of H(BA) with O(MeOH) that is located at 1.7 Å, a distance typical for a strong hydrogen bond. The peak decreases from a value of about 190 at 12 MPa to 160 at 28 MPa. Another H-bonding peak with a height of ≈20 is observed at 1.9 Å involving H(MeOH) as the donor and the carbonyl O(BA) as the acceptor. Almost nonexistent are H-bonding interactions between H(MeOH) and hydroxyl O(BA) with a peak height of ≈1.5. The corresponding number integrals show coordination numbers at r = 2.5 Å of 0.8, 0.2, and 0.02, respectively. This pattern of interactions follows the strength of the respective interactions. The TraPPE force field assigns a partial charge of $-0.7e$ to the MeOH oxygen atom, while the OPLS carboxylic acid has charges of $-0.53e$ and $-0.44e$ on the hydroxyl and carbonyl oxygens, respectively. The hydrogen atom has a charge of $+0.435e$ and $+0.45e$ in the MeOH and BA molecules, respectively. As a result of the larger partial charge on the alcohol oxygen atom, interactions between this site and the acid hydroxyl hydrogen are stronger than those

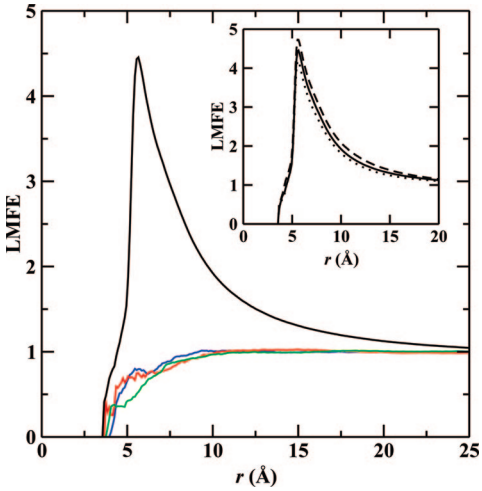

Figure 6. Local mole fraction enhancements of entrainer molecules around solute molecules in the SC phase at $p^{ext} = 20$ MPa. The blue, red, green, and black lines illustrate OCT around HMB, MeOH around HMB, OCT around BA, and MeOH around BA, respectively. The inset shows the effect of pressure on the LMFE for MeOH around BA at 12 MPa (dashed), 20 MPa (solid), and 28 MPa (dotted).

involving the alcohol hydrogen atom. The partial charges on the two BA oxygen atoms are similar, but the carbonyl oxygen atom is more exposed. This allows a methanol molecules that already accepts an H-bond from BA to donate a second H-bond to the carbonyl oxygen or for other methanol molecules to donate to the carbonyl oxygen. A more detailed analysis of H-bonding and aggregate formation is provided below.

It should be noted here that the partial charges for the MeOH and BA molecules reflect the enhanced charge distribution present in liquid phase of these compounds.[36,39] To some extent, one may expect less hydrogen bonding and, hence, somewhat smaller magnitudes of the partial charges for the SC phases. This may be the reason that the CISE for BA in SC-CO_2/MeOH found in the simulations exceeds the experimental value. However, the TraPPE force field yields very satisfactory agreement for the binary phase diagram of MeOH and CO_2,[14] and simulations for a polarizable force field would be significantly more expensive.[58]

D. Preferential Solvation. One proposed mechanism[59] for the solubility enhancement seen in CO_2/entrainer systems, particularly in systems with polar entrainers and polar solutes, is preferential solvation of the solute molecules. The entrainers may cluster around the solute forming a more favorable local environment compared to the bulk solvent. In order to examine this effect, the local mole fraction enhancement (LMFE) of the entrainer species around the solute molecules was calculated from the NIs for center-of-mass RDFs. The local mole fraction is defined as

$$x_A(r) = \frac{N_A(r)}{N_{CO_2}(r) + N_{entrainer}(r) + N_{solute}(r)} \quad (4)$$

where $N_A(r)$ is the average number of neighbors of type A within a sphere of radius r around a solute molecule. This value is normalized by the bulk mole fraction of A to determine the LMFE. These are depicted in Figure 6 for the entrainers around the solute molecules for each system at 20 MPa. With the exception of MeOH around BA, the LMFE do not show any enhancements (values greater than unity); i.e., there is no enrichment of OCT around these solutes. In contrast, there is a more than 4-fold enhancement for MeOH around BA that is sharply peaked at $r = 5.6$ Å, but with an extended tail at large separations, e.g., an LMFE of 1.1 at $r \approx 21$ Å. The LMFEs do not depend strongly on p^{ext}; even the decrease in the LMFE for MeOH around BA with increasing p^{ext} is very small, changing from 4.7 to 4.2 as p^{ext} is increased from 12 to 28 MPa (see inset of Figure 6). It should be noted here that the LMFE is necessarily defined based on center-of-mass separations (and not on site−site separations of molecular fragments); thus, the intramolecular separation of the carboxylic group from the COM of BA disfavors a close approach of the MeOH and BA centers of mass, whereas a small fraction of CO_2 molecules is found close to the phenyl ring and, hence, BA's COM.

TABLE 3: Fraction of BA Molecules Participating in a Given Number of Hydrogen Bonds in the SC-CO_2/MeOH Phase As a Function of p^{ext} [a]

no. of hydrogen bonds	12 MPa	20 MPa	28 Mpa
0	0.08_1	0.11_1	0.12_1
1	0.60_3	0.59_4	0.59_1
2	0.31_3	0.29_3	0.28_1
≥3	0.010_1	0.009_3	0.006_3

[a] Subscripts denote the standard error of the mean.

E. Hydrogen Bonding. The significant LMFE for MeOH around BA arises primarily due to specific H-bond interactions. Here, a hydrogen bond is considered to exist between two molecules if the following criteria are satisfied:[60] $r_{OO} \leq 3.3$ Å, $r_{HO} \leq 2.5$ Å, and $\cos \theta_{OH\cdots O} < -0.4$. On average, approximately 92, 89, and 88% of the BA molecules in the SC phase are involved in at least one H-bond at $p^{ext} = 12$, 20, and 28 MPa, respectively (see Table 3). Of these H-bonded solute molecules, about two-thirds participate in only one hydrogen bond, primarily with a MeOH molecule (95%), while the remainder participate in at least two hydrogen bonds. These primarily involve two MeOH molecules, although some aggregates containing more than one solute molecule or with multiple hydrogen bonds between two molecules are present. There are on average 1.20 ± 0.04 hydrogen bonds for each BA molecule in SC-CO_2/MeOH at $p^{ext} = 20$ MPa. The slightly smaller fraction of BA molecules not associated in H-bonds with MeOH and the slightly larger LMFE observed at $p^{ext} = 12$ MPa is the likely reason for the larger CISE observed at this pressure.

Figure 7 illustrates the size distribution for BA/MeOH aggregates at all three pressures. The data were normalized by the total number of solute molecules in the SC phase. With the exception of the isolated BA molecules, the aggregate size distribution is relatively insensitive to pressure. At $p^{ext} = 20$ MPa, the majority of BA molecules are present in aggregates consisting of two or three molecules, 35% or 24%, respectively, and an additional 14% are found in tetrameric aggregates. The remaining 16% of BA molecules are found in larger aggregates. Primarily, the aggregates form with one BA molecule and one or more MeOH molecules. A small fraction of isolated BA dimers is present (1% of the two-molecule aggregates at 20 MPa), and larger aggregates are more likely to contain more than one BA molecule. In contrast to the strong aggregation found in SC-CO_2 with MeOH entrainer, aggregations plays only a minor role for solvation in SC-CO_2 without an entrainer. At $p^{ext} = 20$ MPa, 87 ± 2% of BA molecules in SC-CO_2 do not participate in any H-bond.

Dimerization plays an important role for the properties of the saturated vapor phase of low-molecular-weight carboxylic acids. However, it is less prevalent for high-molecular-weight carboxylic acids at room temperature because the dramatic

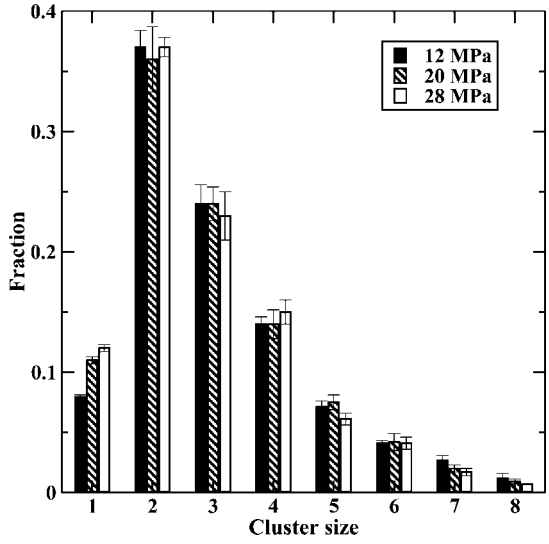

Figure 7. Aggregate size distributions for BA-containing, hydrogen-bonded clusters in SC-CO_2/MeOH normalized by the number of solute molecules in the SC phase. Error bars indicate standard error of the mean over four independent simulations.

decrease in vapor pressure with molecular weight leads to an increase in the entropic penalty associated with dimerization. Indeed, the overwhelming majority of BA molecules is found as isolated monomers in the vapor phase at all three Poynting-corrected pressures. The equilibrium constant (K_{eq}) for BA dimerization is given by

$$2C_6H_5COOH \rightleftharpoons (C_6H_5COOH)_2 \qquad K_{eq} = \frac{\rho_{(C_6H_5COOH)_2}}{(\rho_{C_6H_5COOH})^2} \tag{5}$$

For BA solvated in SC-CO_2/MeOH, the concentration of BA monomers and BA dimers may be defined in different manners. In one case, only isolated species may be considered; i.e., there are no additional MeOH molecules that H-bond to either BA monomer or dimer. Alternatively, BA monomers and dimers may be solvated. In this case, any aggregate that contains only one BA molecule is considered a monomer, even if the BA molecule participates in H-bonds with MeOH. Similarly, dimers are defined as H-bonded aggregates of MeOH and BA that contain exactly two BA molecules irrespective of whether there is a direct H-bond between the two BA molecules. At $p^{ext} =$ 20 MPa, about 16% of the BA monomers and only 3% of the BA dimers are found as isolated species. Averaging over the three pressures, the simulations yield K_{eq} values of 4.7 ± 1.1, 3.1 ± 0.7, and 1.5 ± 0.1 (molecules/nm^3)$^{-1}$ for the SC-CO_2 phase, for isolated species and for all species in the SC-CO_2/MeOH, respectively. Thus, the presence of MeOH shifts the equilibrium toward the monomer side (or, aggregates that contain only one BA molecules), and, most importantly, increases the overall number density of BA moelcules in the SC phase by an order of magnitude.

An analysis of the H-bonding of aggregates containing two BA molecules shows that there is no statistically significant difference in the H-bonding for BA dimers in SC-CO_2 and isolated dimers in SC-CO_2/MeOH (see Table 4). In both cases, about 1.4 H-bonds are found per dimer and about 40% of the dimers are connected by two H-bonds. The number of BA-BA H-bonds is reduced by a factor of 3 to 0.45 when all aggregates containing two BA molecules in SC-CO_2 are considered. In this case, only 1% of these aggregates contain BA molecules that are connected to each other by two H-bonds, whereas the majority contains BA molecules that do not H-bond to each other, i.e., that are connected through a MeOH bridge.

TABLE 4: Hydrogen-Bond Analysis for BA Dimers in the SC Phase at $p^{ext} = 20$ MPa: BA Number Density (in units of molecules/nm^3), Numbers of H-Bonds between BA Molecules and with MeOH Molecules, and Fractions of Aggregates That Contain BA Molecules That Are Connected to Each Other by Two, One, and Zero H-Bonds[a]

system	ρ_{BA}		H_{BA}	H_{MeOH}	$f_{2\,BAHB}$	$f_{1\,BAHB}$	$f_{0\,BAHB}$
CO_2	0.019_2		1.39_8	—	0.39_{16}	0.61_{16}	—
CO_2/MeOH	0.233_7	isolated	1.35_8	—	0.35_{14}	0.65_{14}	—
		all	0.45_3	2.37_6	0.01_1	0.43_7	0.55_7

[a] Subscripts denote the standard error of the mean.

5. Conclusions

The effects of increasing the applied pressure and adding entrainers on the solubilities of hexamethylbenzene and benzoic acid in supercritical CO_2 were investigated via molecular simulation. It is demonstrated that the Poynting correction, i.e., the increase in the solid's vapor pressure with increasing applied pressure, is the most important factor leading to an increase in solubility, while solvent density effects are of minor importance for solvation in neat supercritical CO_2. In other words, an increase in the applied pressure mostly "tunes" the chemical potential of the solute and not the solvent strength of neat supercritical CO_2 for the systems investigated here.

The presence of *n*-octane and methanol entrainers leads to an increase in solubility for the low-volatility solutes, particularly when the polarity of the entrainer and solute are similar. When the entrainer is nonpolar, the increase in solubility arises from weak attractive forces more than any pronounced change in the solvent's structure. In contrast, preferential solvation of benzoic acid by methanol, via the formation of hydrogen-bonded aggregates, is the driving force for the dramatically enhanced solubility for this solute−entrainer combination in supercritical CO_2. In SC-CO_2/MeOH, most of the BA molecules form hydrogen bonds to MeOH and the equilibrium constant for the formation of aggregates containing two BA molecules is shifted toward the monomer side compared to solvation in SC-CO_2. Further understanding of the molecular-level effects of entrainer addition to supercritical fluids may allow for tuning of the selectivity of solvent−entrainer systems which would have implications for a wide range of applications.

Acknowledgment. We thank M. Greenfield for very helpful conversations regarding the Poynting correction. Financial support from the National Science Foundation (CBET-0553911) and Louise Dosdall and 3M Science and Technology Graduate Fellowships (KEA) is gratefully acknowledged. Part of the computer resources were provided by the Minnesota Supercomputing Institute.

References and Notes

(1) Hannay, J. B.; Hogarth, J. *Proc. R. Soc. London* **1879**, *29*, 324.
(2) Eckert, C. A.; Knutson, B. L.; Debenedetti, P. G. *Nature* **1996**, *383*, 313.
(3) McHugh, M. A.; Krukonis, V. J. *Supercritical Fluid Extraction: Principles and Practice*, 2nd ed.; Butterworth: Boston, 1994.
(4) Taylor, L. T. *Supercritical Fluid Extraction*; Wiley: New York, 1996.
(5) Dobbs, J. M.; Wong, J. M.; Johnston, K. P. *J. Chem. Eng. Data* **1986**, *31*, 303.

(6) Dobbs, J. M.; Wong, J. M.; Lahiere, R. J.; Johnston, K. P. *Ind. Eng. Chem. Res.* **1987**, *26*, 56.
(7) Brennecke, J. F.; Eckert, C. A. *AIChE J.* **1989**, *35*, 1409.
(8) Chialvo, A. A.; Debenedetti, P. G. *Ind. Eng. Chem. Res.* **1992**, *31*, 1391.
(9) Inomata, H.; Saito, S.; Debenedetti, P. G. *Fluid Phase Equilib.* **1996**, *116*, 282.
(10) Tucker, S. C. *Chem. Rev.* **1999**, *99*, 391.
(11) Maddox, M. W.; Goodyear, G.; Tucker, S. C. *J. Phys. Chem. B* **2000**, *104*, 6248.
(12) Vorholz, J.; Harismiadis, V. I.; Rumpf, B.; Panagiotopoulos, A. Z.; Maurer, G. *Fluid Phase Equilib.* **2000**, *170*, 203.
(13) Chatzis, G.; Samios, J. *Chem. Phys. Lett.* **2003**, *374*, 187.
(14) Stubbs, J. M.; Siepmann, J. I. *J. Chem. Phys.* **2004**, *121*, 1525.
(15) Skarmoutsos, I.; Samois, J. *J. Mol. Liq.* **2006**, *125*, 181.
(16) Skarmoutsos, I.; Dellis, D.; Samois, J. *J. Chem. Phys.* **2007**, *126*, 224503.
(17) Saharay, M.; Balasubramanian, S. *J. Phys. Chem. B* **2007**, *111*, 387.
(18) Shing, K. S.; Chung, S. T. *J. Phys. Chem.* **1987**, *91*, 1674.
(19) Eya, H.; Iwai, Y.; Fukuda, T.; Arai, Y. *Fluid Phase Eq.* **1992**, *77*, 39.
(20) Iwai, Y.; Mori, Y.; Koga, Y.; Arai, Y.; Eya, H. *J. Chem. Eng. Jpn.* **1994**, *27*, 334.
(21) Iwai, Y.; Koga, Y.; Hata, Y.; Uchida, H.; Arai, Y. *Fluid Phase Equilib.* **1995**, *104*, 403.
(22) Iwai, Y.; Uchida, H.; Koga, Y.; Mori, Y.; Arai, Y. *Fluid Phase Equilib.* **1995**, *111*, 1.
(23) Iwai, Y.; Uchida, H.; Arai, Y.; Mori, Y. *Ind. Eng. Chem. Res.* **1996**, *35*, 3782.
(24) Koga, Y.; Iwai, Y.; Yamamoto, M.; Arai, Y. *Fluid Phase Equilib.* **1997**, *131*, 83.
(25) Iwai, Y.; Uchida, H.; Arai, Y.; Mori, Y. *Fluid Phase Equilib.* **1998**, *144*, 233.
(26) Agrawal, P. M.; Sorescu, D. C.; Rice, B. M.; Thompson, D. L. *Fluid Phase Equilib.* **1999**, *155*, 177.
(27) Agrawal, P. M.; Rice, B. M.; Sorescu, D. C.; Thompson, D. L. *Fluid Phase Equilib.* **2001**, *187*−*188*, 139.
(28) Albo, S.; Müller, E. A. *J. Phys. Chem. B* **2003**, *107*, 1672.
(29) Su, Z.; Maroncelli, M. *J. Chem. Phys.* **2006**, *124*, 164506.
(30) Nouacer, M.; Shing, K. S. *Mol. Simul.* **1989**, *2*, 55.
(31) Agrawal, P. M.; Rice, B. M.; Sorescu, D. C.; Thompson, D. L. *Fluid Phase Equilib.* **1999**, *166*, 1.
(32) Iwai, Y.; Mori, Y.; Arai, Y. *Fluid Phase Equilib.* **2000**, *167*, 33.
(33) Higashi, H.; Iwai, Y.; Arai, Y. *Chem. Eng. Sci.* **2001**, *56*, 3027.
(34) Martin, M. G.; Siepmann, J. I. *J. Phys. Chem. B* **1998**, *102*, 2569.
(35) Potoff, J. J.; Siepmann, J. I. *AIChE J.* **2001**, *47*, 1676.
(36) Chen, B.; Potoff, J. J.; Siepmann, J. I. *J. Phys. Chem. B* **2001**, *105*, 3093.
(37) Wick, C. D.; Martin, M. G.; Siepmann, J. I. *J. Phys. Chem. B* **2000**, *104*, 8008.
(38) TraPPE Force Field; http://www.chem.umn.edu/groups/siepmann/trappe/intro.php (accessed on March 14, 2008).
(39) Jorgensen, W. L.; Maxwell, D. S.; Tirado-Rives, J. *J. Am. Chem. Soc.* **1996**, *118*, 11225.
(40) Chen, B.; Siepmann, J. I.; Klein, M. L. *J. Phys. Chem. B* **2001**, *105*, 9840.
(41) (a) Lorentz, H. A. *Ann. Phys.* **1881**, *12*, 127. (b) Berthelot, D. *C. R. Hebd. Séanc. Acad. Sci., Paris* **1898**, *126*, 1703.
(42) Allen, M. P.; Tildesley, D. J. *Computer Simulation of Liquids*; Oxford University Press: Oxford, UK, 1987.
(43) Panagiotopoulos, A. Z. *Mol. Phys.* **1987**, *61*, 813.
(44) Panagiotopoulos, A. Z. *Mol. Phys.* **1987**, *62*, 701.
(45) Panagiotopoulos, A. Z.; Quirke, N.; Stapleton, M.; Tildesley, D. J. *Mol. Phys.* **1988**, *63*, 527.
(46) Smit, B.; de Smedt, P.; Frenkel, D. *Mol. Phys.* **1989**, *68*, 931.
(47) Wick, C. D.; Siepmann, J. I.; Sheth, A. R.; Grant, D. W. R.; Karaborni, S. *Cryst. Growth Des.* **2006**, *6*, 1318.
(48) Siepmann, J. I.; Frenkel, D. *Mol. Phys.* **1992**, *75*, 59.
(49) Martin, M. G.; Siepmann, J. I. *J. Phys. Chem. B* **1999**, *103*, 4508.
(50) McDonald, I. R. *Mol. Phys.* **1972**, *23*, 41.
(51) Chen, B.; Siepmann, J. I. *J. Phys. Chem. B* **2000**, *104*, 8725.
(52) Chen, B.; Siepmann, J. I. *J. Phys. Chem. B* **2001**, *105*, 11275.
(53) Ambrose, D.; Lawrence, I. J.; Sprake, C. H. S. *J. Chem. Thermodyn.* **1976**, *8*, 503.
(54) Colomina, M.; Jimenez, P.; Turrion, C. *J. Chem. Thermodyn.* **1982**, *14*, 779.
(55) Prausnitz, J. M.; Lichtenthaler, R. N.; Gomes de Azevedo, E. *Molecular Thermodynamics of Fluid-Phase Equilibria*, 3rd ed.; Prentice Hall: Englewood Cliffs, NJ, 1999.
(56) Press, W. L.; Flannery, B. P.; Teukolsky, S. A.; Wetterling, V. T. *Numerical Recipes in Fortran 77*; 2nd ed.; Cambridge University Press: Cambridge, UK, 1992.
(57) Martin, M. G.; Chen, B.; Siepmann, J. I. *J. Phys. Chem. B* **2000**, *104*, 2415.
(58) Chen, B.; Potoff, J. J.; Siepmann, J. I. *J. Phys. Chem. B* **2000**, *104*, 2378.
(59) Johnston, K. P.; Kim, S.; Combes, J. Spectroscopic Determination of Solvent Strength and Structure in Supercritical Fluid Mixtures: A Review. In *Supercritical Fluid Science and Technology*; Johnston, K. P., Penninger, J. M. L. Eds.; American Chemical Society: Washington, DC, 1989; pp 52−70.
(60) Stubbs, J. M.; Siepmann, J. I. *J. Phys. Chem. B* **2002**, *106*, 3968.

JP802374C